INSIGHT INTO THE CORROSION AND FILMING BEHAVIOUR OF ALUMINIUM AND ITS ALLOYS

X SUN*, X ZHOU*, G E THOMPSON*, P SKELDON*, K SHIMIZU, R C FURNEAUX*** and G SCAMANS*****

* Corrosion and Protection Centre, UMIST, PO Box 88, Manchester, M60 1QD, England
** University Chemical Laboratory, Keio University, 4-1-1 Hiyoshi, Yokohama 223, Japan
*** Alcan International Ltd, Southam Road, Banbury, Oxon, OX16 7SP, England

ABSTRACT Consideration is given to the effects of alloying aluminium on the subsequent corrosion and filming behaviour. With regard to deliberate filming by anodic oxidation, the effects of alloying elements in solid solution can be quantified from consideration of the Gibbs free energy for oxide formation per equivalent relative to that of alumina and, where appropriate, the metal-oxygen bond strength and Pilling-Bedworth rate for oxide formation. With regard to corrosion behaviour during alloy pretreatment, the effects of alloying elements present as fine precipitates,or coarse second phase, can be determined by a combined TEM and AFM approach, allowing precise quantification of local and general corrosion rates. Finally, the influence of alloy composition and thermomechanical processing on performance may be very marked in particular circumstances.

Keywords: *aluminium, alloying, second phase, filming, corrosion*

1. INTRODUCTION

Aluminium, in pure and alloyed forms, is used widely in many application areas, ranging from architecture through capacitors to transport. A key feature of its successful, widespread exploitation is the presence of the air-formed alumina film over the macroscopic aluminium surface, which limits environmental access to the substrate to flawed or defect regions. Further, the air-formed film is reactive in various environments, transforming to passive films or to residual alumina films which are sandwiched between the substrate and some outer film region, ie conversion coating. In transformations of the previous kinds, the anodic reaction is oxidation of aluminium to amorphous alumina, with the outer film regions dissolving in the reactive electrolyte; clearly the anodic process is supported by a cathodic process, located at impurity segregation, second phase etc. Concerning ultra high purity aluminium, which is devoid of sufficient impurity segregates and second phase material, the transformation of the original air-formed film results in a suitably thinned, residual alumina film that allows electron tunnelling. Thus, depending on material and environment, cathodic sites may be activated at various locations over the filmed aluminium surface. Concerning anodic oxidation per se, usually carried out galvanostatically to develop alumina films at high current efficiency, this involves ionic transport of Al^{3+} ions and O^{2-} ions across the thickening alumina under a high field, with film growth at the film/electrolyte and aluminium/film interfaces respectively.

Using information of the previous kind, the corrosion and filming behaviour of aluminium and selected alloys have been examined, with effects at the matrix and segregates or second phase examined and their zones of influence probed.

2. EXPERIMENTAL

General information is provided here, with specific details given, where appropriate, in later sections. For observation of aluminium and its alloys, transmission electron microscopy of ultramicrotomed sections was undertaken. The electron transparent sections included the original aluminium and its alloys or the substrate supporting its anodic film. In the former case, the sections were used to reveal aluminium grains, grain boundaries, fine precipitates and relatively coarse second phase material, with appropriate EDX analyses. Ultramicrotomed sections of the aluminium and its anodic film were generated by sectioning parallel to the metal/film interface. In all cases the specimens were trimmed initially with glass knives and final sections were generated with a diamond knife; specimens were observed routinely in a JEOL 2000 FX II instrument with STEM and EDX facilities.

Important topographical information was probed by atomic force microscopy of suitably flat specimens; such specimens, of typical roughness < 1nm, were generated by ultramicrotomy, with the ultramicrotomed slice used for TEM and the remaining specimen block used for AFM. In order to examine electrolyte interactions with the respective specimens, the ultramicrotomed sections were allowed to 'float' on the solution after cutting, whereas the block was immersed in the solution. AFM was undertaken in a Digital Instruments Nanoscope III, in the tapping mode, using a Si_3N_4 tip and a 125 μm, length cantilever of spring constant 16-73 Nm^{-1} and resonant frequency of 242-396 kHz

Where appropriate, Rutherford backscattering spectroscopy was undertaken, using a 2.0 MeV alpha particle beam produced by the Van de Graaff facility at the University of Paris.

3. RESULTS

3.1 Alloy Matrix Effects During Anodic Oxidation

Table 1 records the Gibbs free energies of oxide formation per equivalent ($\Delta G^o/n$) of alloying

Table 1. Gibbs free energies of oxide formation per equivalent for various alloying elements (The shaded regions represent alloying elements that have not been examined to date.)

Element	Oxide	$\Delta G^o/n$(kJ mol^{-1})	Element	Oxide	$\Delta G^o/n$(kJ mol
Al	Al_2O_3	-263.7	Li		-280.6
Ag	Ag_2O	-15.6	Mg		-284.7
B	B_2O_3	-199.1	Mn		-181.5
Ba	BaO	-262.6	Mo		-111.3
Bi	Bi_2O_3	-82.3	Nb		-176.6
Ca	CaO	-301.7	Sn		-129.0
Cd	CdO	-114.4	Si		-214.1
Ce	CeO_2	-256.2	Sm		-289.1
Cr	Cr_2O_3	-176.4	Ta		-191.1
Cu	CuO	-64.9	Ti		-222.2
Fe	Fe_2O_3	-123.7	V		-142.0
Ga	Ga_2O_3	-166.4	W		-127.3
In	In_2O_3	-68.8	Zn		-160.3

elements in aluminium of thickness 1-5 nm, immediately beneath the anodic film formed in ammonium pentaborate electrolyte at 5 mA cm^{-2}. A good correlation is revealed between extent of enrichment, ie number of alloying element atoms contained in an enriched region, and the Gibbs free energy of oxide formation per equivalent. Thus, alloying elements with $\Delta G^{\circ}/n$ values greater than that for alumina reveal interfacial enrichment; for such alloying elements, enrichment proceeds to a steady-state level whilst the anodic alumina film thickens. Upon attainment of a critical enrichment level, appropriate alloying elements are oxidized at the alloy/film interface and are incorporated within the alumina film in their alloying proporitons, with the enriched layer maintaining its critical concentration. Upon incorporation, the oxidized alloying element species, may be immobile or mobile outwards, with migration rates similar to, or less than that of Al^{3+} ions. Calculation of the single metal-oxygen bond strength relative to that of alumina gives an initial indication of the relative mobility with respect to outwardly mobile Al^{3+} ions.

For alloying elements with $\Delta G^{\circ}/n$ values less than alumina, eg Li, Mg and rare earth elements, no initial enrichment is evident. Thus, cerium, for example, is oxidized immediately at the alloy/film interface and is incorporated into the anodic alumina in its alloying proportions. Further, the oxidized cerium species have greater outward mobility than Al^{3+} ions and form an outer cerium-rich oxide layer above the cerium-doped alumina layer. For lithium and magnesium containing alloys, similar processes occur to those for the Al-Ce alloys except, under the anodizing conditions employed, oxidized lithium or magnesium species are ejected directly to the electrolyte from the film/solution interface. Interestingly, anodic oxidation of Al-Li and Al-Mg alloys is also associated with film detachment which, for Al-Mg alloys is associated with fine voidage close to the alloy/film interface. Such voidage is considered to result from the low Pilling Bedworth ratio of anodic magnesium oxide and, possibly, the relatively high mobility of Mg^{2+} ions relative to that of Al^{3+} ions.

Knowledge of the previous kind has immediate relevance to surface treatment of aluminium containing low levels of alloying elements, ie copper. Through pretreatment and anodizing for capacitor applications, copper will enrich at the metal/film interface. Additionally, of practical relevance, synergistic effects are evident between alloying elements in ternary alloys; thus, film detachment is not revealed in Al-Mg alloys with additions of copper. Figure 1 shows a ternary Al-Cu-Au alloy, produced by magnetron sputtering; after anodizing to 25 V, both copper and gold have

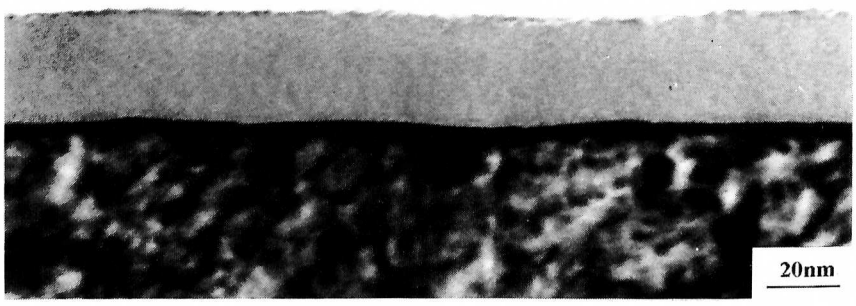

Figure 1. **Transmission electron micrograph of an ultramictromed section of the film formed on an Al-Cu-Au alloy; interfacial enrichment is evident in the alloy.**

enriched substantially, but no oxidation of copper has yet proceeded; oxidation of copper is readily detected by development of oxygen-filled bubbles within the alumina film as a result of the semiconducting nature of the Cu-O bond.

3.2 Effects of Second Phase Material

Relatively coarse second phase material, as well as fine strengthening precipitates, can have various influence on the corrosion and filming behaviour of aluminium. Thus, during anodizing, θ precipitates have been shown to contribute to the enhanced porosity of anodic films through oxygen gas evolution at the interface with the anodic film, subsequent film rupture, electrolyte access and precipitate dissolution and finally reanodizing. Further, depending largely on the composition of second phase material, it may be oxidized fully during anodizing (Al_3Fe) or partially oxidized (Al_6Fe) and occluded in the developing porous anodic alumina film. Behaviour of the previous kind is reasonably well understood from examination of binary solid solution alloys, where enrichment proceeds prior to oxidation and incorporation of alloying element species into the thickening oxides. Thus, for θ′ precipitates, the copper content is close to the critical enrichment level such that copper and aluminium are oxidized almost immediately; oxygen gas generation results from the creation of conducting Cu-O oxide units. For $FeAl_3$ and $FeAl_6$, differing extents of enrichment precede oxidation of the alloying element and incorporation into the oxide.

With regard to the corrosion behaviour of aluminium, for example in deionized water and as a result of pretreatment prior to finishing operation, varied behaviour is evident. For example $FeAl_3$ has been shown to be an effective cathode, with development of local alkalinity which contributes to the anodic dissolution of the adjacent, alumina-filmed matrix. Conversley, Al_6Fe particles are relatively inert under such situations. Given the apparently inert nature of $FeAl_6$ particles, their presence can be used to quantify the dissolution of the matrix in acid pickling, for example. Figure 2 shows an AFM image of a binary Al-Fe alloy, with Al_6Fe particles present at grain boundaries.

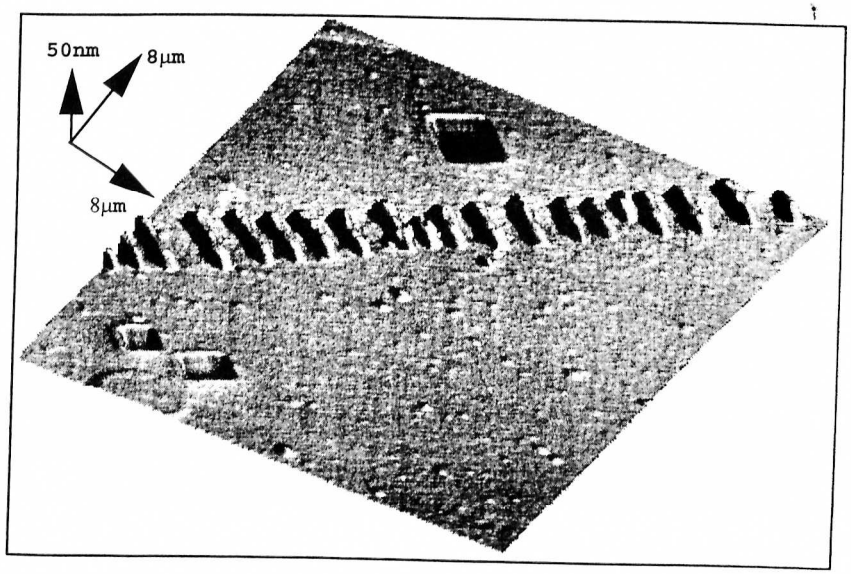

Figure 2. AFM image of an Al-Fe alloy after acid pickling; Al_6Fe particles are revealed.

As a result of acid dissolution, the matrix around the particles has receeded; such recession can be quantified readily in the topographic images, revealing a corrosion rate of 6 nm min^{-1} in acid solution. In the previous case, the specimens were generated by ultramicrotomy, with the electron transparent sections used for TEM and the specimen block utilised for AFM, the block has a roughness less than 1 nm over very significant areas, making it ideal for probing topography at the nanometre level.

With regard to TEM, Figure 3a reveals an AlFeMnSi particle in the matrix of a 5000 series alloy;

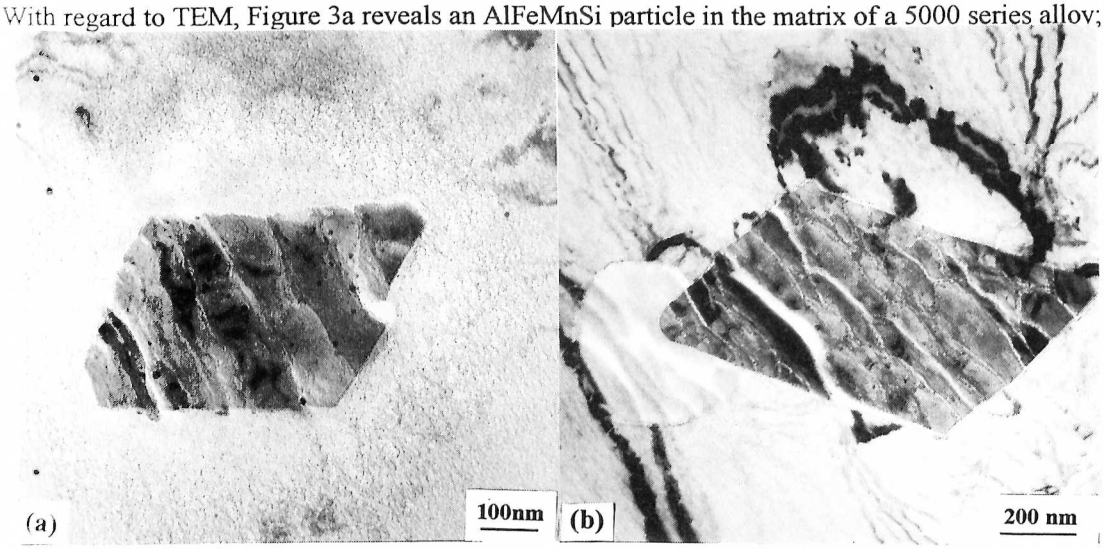

Figure 3. **Transmission electron micrographs of ultramicrotomed sections of a 5000 series alloy: (a) AlFeMnSi particle and asssociated corrosion; (b) AlFeMnSi and Mg_2Si particles, with no evidence of corrosion.**

as a result of exposure to 0.5 M NaCl solution, localised corrosion has occurred in the matrix close to the particles. Thickness variations across the section can be determined readily by TEM/EELS, thus quantifying localised corrosion rates. The micrograph of Figure 3b reveals a similar particle, plus an Mg_2Si particle, after immersion in Cl^-/CrO_4^{2-} solution; in this case little or no corrosion is evident, consistent with the presence of Cr^{6+} species. Again, metal loss can be quantified by EELS which may also be used as a probe for chromium species; from Figure 3b, significant chromium species are associated with the particles and immediately adjacent matrix. From scrutiny of the chromium and oxygen edges, possible differentiation between the oxidation states of chromium specimen is being explored.

3.3 Alloy Processing

In addition to the effects highlighted previously, i.e. interfacial processes associated with alloying elements and local processes associated with alloying elements in the form of second phase material, the processing of aluminium alloys may result in very significant alteration of the near surface layers. The presence of fine (submicron) grain structures, i.e. through intense plastic strain, is well known; however, the presence of altered regions, with grain boundaries decorated by oxide, persisting through hot and cold rolling to produce final sheet, with consequent effects on alloy performance, is recently being quantified. Figure 4 shows a section of the near surface region of a 5000 series alloy; an altered region of thickness up to 1 μm is revealed. Further, such regions are not removed uniformly by acid pickling (Figure 4b), which penetrates the layers locally; finally, after removal of such layers by grinding, limited heating may promote their reappearance. Such

layer development is the subject of on-going studies, with inter-relationships between form conditions and alloy content being developed.

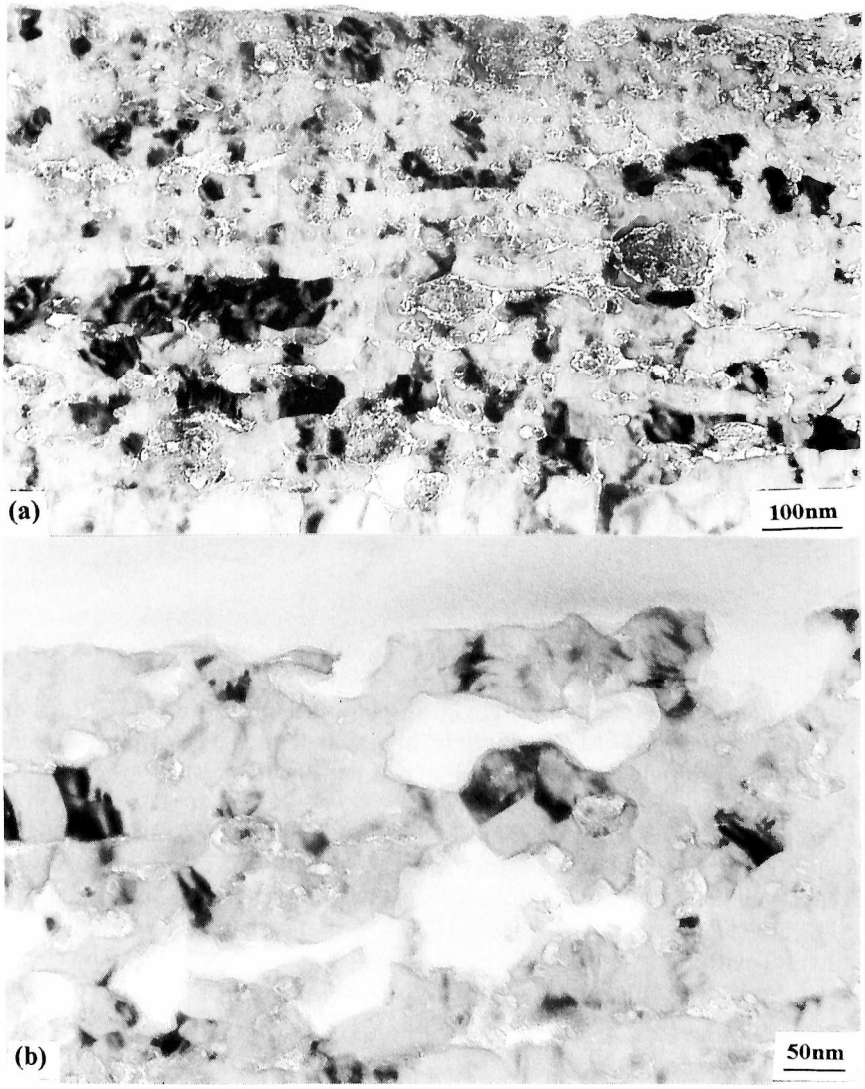

Figure 4. **Transmission electron micrographs of ultramicrotomed sections of a 5000 seri alloy; (a) in final sheet form, revealing altered surface layers; (b) as (a) bu after acid pickling.**

4. SUMMARY

The general and local behaviour of aluminium alloys under various circumstances can be prob readily by TEM with EDX and EELS, with further quantification through topographical probing b AFM. Varied behaviour of individual alloying elements is revealed, with synergistic effects show by combinations of alloying elements.

k:\text\get\papers\insight2538.cc